

Orbital angular momentum based *intra*- and *inter*- particle entangled states generated via a quantum dot source

Alessia Suprano,¹ Danilo Zia,¹ Mathias Pont,² Taira Giordani,¹ Giovanni Rodari,¹ Mauro Valeri,¹ Bruno Piccirillo,^{3,4} Gonzalo Carvacho,¹ Nicolò Spagnolo,¹ Pascale Senellart,² Lorenzo Marrucci,³ and Fabio Sciarrino^{1,*}

¹*Dipartimento di Fisica, Sapienza Università di Roma, Piazzale Aldo Moro 5, I-00185 Roma, Italy*

²*Centre for Nanosciences and Nanotechnology, CNRS, Université Paris-Saclay, UMR 9001, 10 Boulevard Thomas Gobert, 91120, Palaiseau, France*

³*Dipartimento di Fisica "Ettore Pancini", Università di Napoli Federico II, Complesso Universitario di Monte Sant'Angelo, Via Cintia, 80126 Napoli, Italy*

⁴*INFN – Sezione di Napoli, Via Cintia, 80126 Napoli, Italy*

Engineering single-photon states endowed with Orbital Angular Momentum (OAM) is a powerful tool for quantum information photonic implementations. Indeed, thanks to its unbounded nature, OAM is suitable to encode qudits allowing a single carrier to transport a large amount of information. Nowadays, most of the experimental platforms use nonlinear crystals to generate single photons through Spontaneous Parametric Down Conversion processes, even if this kind of approach is intrinsically probabilistic leading to scalability issues for increasing number of qudits. Semiconductors Quantum Dots (QDs) have been used to get over these limitations being able to produce on demand pure and indistinguishable single-photon states, although only recently they were exploited to create OAM modes. Our work employs a bright QD single-photon source to generate a complete set of quantum states for information processing with OAM endowed photons. We first study the hybrid *intra*-particle entanglement between the OAM and the polarization degree of freedom of a single-photon. We certify the preparation of such a type of qudit states by means of the Hong-Ou-Mandel effect visibility which furnishes the pairwise overlap between consecutive OAM-encoded photons. Then, we investigate the hybrid *inter*-particle entanglement, by exploiting a probabilistic two qudit OAM-based entangling gate. The performances of our entanglement generation approach are assessed performing high dimensional quantum state tomography and violating Bell inequalities. Our results pave the way toward the use of deterministic sources (QDs) for the on demand generation of photonic quantum states in high dimensional Hilbert spaces.

I. INTRODUCTION

In the last decades, structured light states characterized by an on-demand distribution for both field amplitude and phase have gained great interest [1]. Among them, twisted beams carrying Orbital Angular Momentum (OAM) have been the focus of several studies due to their wide range of applications. As pointed out by Allen *et al.* [2], OAM is carried by all the beams that present a phase term of the form $e^{i\ell\phi}$ where ϕ is the azimuthal angle in cylindrical coordinates and ℓ an unbounded integer. This phase term is responsible for the typical helicoidal wavefront, and each photon shows an OAM equal to $\ell\hbar$.

In classical domain, the non trivial phase structure of OAM states is used in several protocols covering a wide number of fields such as metrology [3], imaging [4–6], particle trapping [7] and communication [8–14]. The unbounded nature of the OAM is instead the basis of its employment in quantum information. Therefore, OAM modes are used in quantum communication [15–20], cryptography [21–23], simulation [24–26], computation and information processing [27–29]. In particular, OAM-based encoding enlarges the amount of information that a single-photon can support, leading to increased security in the communication protocols [30, 31]. When the helicoidal wavefront is coupled with a nontrivial distribution of the Spin Angular Momentum (SAM), also known as polarization, a new class of states called Vector Vortex (VV) is introduced. Given

this peculiar coupling, VV beams turn out to be *intra*-system maximally entangled in the OAM and polarization degrees of freedom. As for the OAM modes, VV beams are applied in several areas both in classical and quantum regime such as optical trapping [32, 33], communication [34, 35], computing [36–44], sensing and metrology [45–49]. Moreover, knowing the importance of the Hong-Ou-Mandel (HOM) effect [50] and its applicability in quantum information science [51], the interference behaviour between structured photons has also been studied in order to perform increasingly complex tasks [52–54].

Despite the large number of applications, sources that produce single photons carrying OAM deterministically and with high brightness are still under development [55]. In fact, most of the experimental implementations leverage on producing single photons through Spontaneous Parametric Down Conversion (SPDC) in nonlinear crystals and modulating their states using bulk systems such as Spatial Light modulators (SLMs) [56, 57] and q-plates [58–60]. However, SPDC is intrinsically probabilistic and suffers from a trade-off between the brightness and the purity of the produced single photons. Moreover, since in each process it is always possible to generate more than one photon, these kinds of sources undermine the security of quantum cryptography schemes [61]. Semiconductor Quantum Dots (QDs) have emerged as a platform to overcome these limitations. Acting as artificial atoms when resonantly pumped with pulsed lasers, QDs are capable of generating indistinguishable single photons with high brightness in a nearly-deterministic fashion [62–65]. However, most of the effort was concentrated on the generation of single or

* fabio.sciarrino@uniroma1.it

entangled states encoding the information in the photons polarization [66–71] or in the temporal domain [72]. Only recently, works exploiting QDs to engineer OAM modes [55] within a prepare-and-measure framework have appeared. In particular, integrated sources based on microring resonators embedded with QDs [55] have been implemented, in which the OAM states encoded in the generated single photons could not be easily manipulated.

At variance with [55], we exploit commercial QD based single-photon sources, and focus on the development of quantum information processing protocols with VV beams. Specifically, well-known OAM manipulation technologies have been extensively used to develop high-dimensional quantum communication protocols [18, 22], to reach a high flexibility in engineering arbitrary qudit states [73, 74], and to develop simulated processes based on the quantum walk dynamics [24, 25]. Here, we combine these technologies with an innovative and nearly deterministic single-photon source, opening the way for further developments of quantum information protocols that take advantage of high-dimensional resources and of the benefits introduced by using QDs. In particular, besides focusing on interfacing between these two kinds of technologies, we perform a step forward and study the hybrid entanglement in high-dimensional Hilbert spaces implementing a quantum gate both in the *intra*- and *inter*- particle regime (Fig. 1). Previously, states characterized by hybrid *intra*-photon entanglement between the OAM and polarization degree of freedom have been generated via SPDC processes [18, 37, 75, 76]. However, since this kind of source is probabilistic, the state is certified in an heralded configuration which drastically decreases the generation rate. On the contrary, the employment of a deterministic single-photon source, allows us to certify the state directly on the single counts increasing the generation rate. Moving toward the *inter*-particle regime, versatility and flexibility in the generation and manipulation of indistinguishable photons are crucial features for gate implementation. We then move a step forward with respect to Ref. [55] by investigating the indistinguishability of the generated photons and employing a versatile approach. In our platform, the combination of QD based single-photon sources and well-known OAM manipulation devices allow us to satisfy the aforementioned requirements.

This work is organized as follows. We start by studying the single-photon *intra*-particle entanglement generation in VV states. By means of q-plate devices [58, 59], we couple the two components of the angular momentum degree of freedom and generate VV beams (Fig. 1-a). Then, we move to the multi-photon scenario. Preliminary, we certify the efficiency of encoding OAM states on single photons emitted by the QD in different pulses of the pump beam through the evaluation of Hong-Ou-Mandel interference visibility. Thus, we implement a 2-photons probabilistic quantum gate able to generate OAM-based entangled photon pairs involving up to 4 subsystems (Fig. 1-b). We verify both the single-photon *intra*-particle and the two-photon entanglement performing quantum state tomography and evaluating the Bell inequality in the Clauser–Horne–Shimony–Holt (CHSH) fashion.

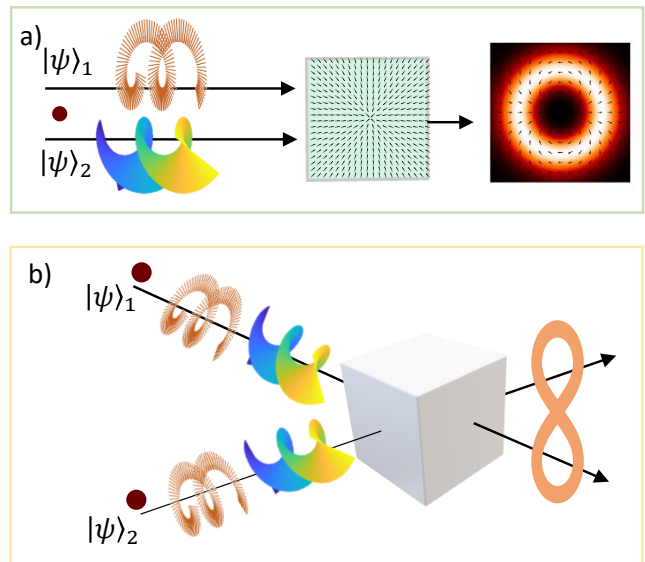


Figure 1. **Entanglement generation.** a) In the *intra*-particle entanglement, the polarization and OAM subsystems are made to interact using a q-plate. The two-dimensional state $|\psi\rangle_1$ is initialized with the right polarization $|R\rangle = |0\rangle$, while the qudit $|\psi\rangle_2$ is prepared with a null OAM value $|0\rangle$. The action of the unitary operator consists of increasing or decreasing the OAM value in a polarization-dependent way. b) In the *inter*-particle regime, two photons characterized by defined states in the hybrid space composed of polarization and OAM interfere using a beam-splitter. Fixing the elements of the computational basis as $|0\rangle = |L, -2\rangle$ and $|1\rangle = |R, 2\rangle$, both $|\psi\rangle_1$ and $|\psi\rangle_2$ are initialized with the qubit state $|0\rangle$, and after post selecting on the coincidence counts a probabilistic entangling quantum gate is implemented. It is worth noting that considering separately the polarization and OAM Hilbert spaces of both photons, the proposed apparatus implements a 4-qubits gate.

II. EXPERIMENTAL PLATFORM

In this section, we preliminarily describe the employed quasi-deterministic single-photon source, evaluating the intensity auto-correlation and indistinguishability of the generated photons. Subsequently, we present the implemented scalable platform in which, by interfacing well-known OAM manipulation devices with the QD source, entangled *intra*- and *inter*-particle states are generated in the hybrid Hilbert space composed of OAM and polarization.

A. Single-photon source

The single-photon source is a quantum dot (QD) based emitter embedded in an electrically controlled cavity on a commercially available *Quandela e-Delight-LA* photonic chip. A single self-assembled InGaAs QD is surrounded by a two Bragg reflectors made of GaAs/Al_{0.95}Ga_{0.05}As $\lambda/4$ layers with 36 (16) pairs for the bottom (top) and positioned in the center of a micropillar [62]. The micropillar is connected to a larger circular

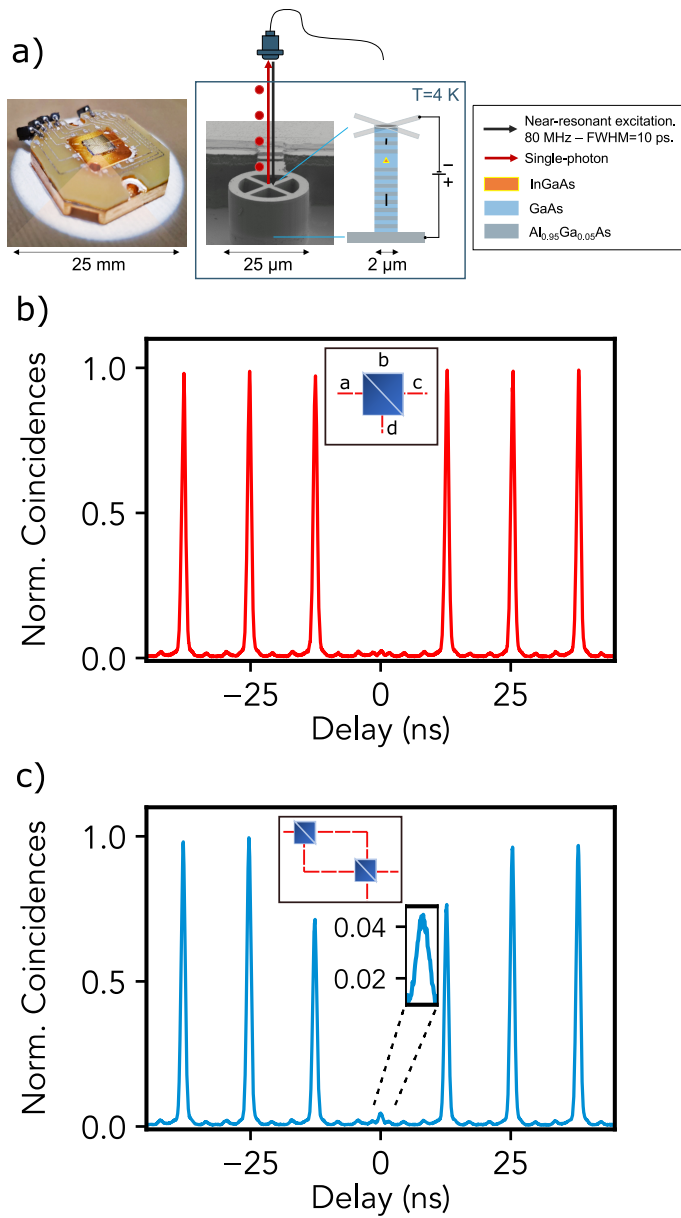


Figure 2. **Source Hong-Ou-Mandel interference and second-order correlation function.** a) The single-photon source (left) is a commercial device (Quandela): InGaAs quantum-dot based bright emitters are embedded in electrically-contacted micropillars (right). The source is pumped with a near-resonant ($\Delta\lambda=-0.6$ nm) FWHM 10 ps 79 MHz-pulsed laser (red arrow). The single photons (red dots) are emitted at a wavelength of 927.8 nm and are directly coupled to a SMF. b) Through a standard Hanbury Brown and Twiss setup, we measure the second-order autocorrelation histogram of our QD-based source as a function of the delay. We obtain a single-photon purity of $g^{(2)}(0) = (1.26 \pm 0.05)\%$. c) Normalized correlation histogram, obtained via a HOM interference experiment, through which we measure an 2-photon interference fringe visibility between subsequent single photons emitted by the QD source of $V_{HOM} = (93.05 \pm 0.06)\%$. Moreover, following Ref. [77], we obtain an indistinguishability value of $M_s = (95.5 \pm 0.1)\%$.

structure that is electrically contacted enabling the tuning of the

emission frequency of the QD with Stark effect. The sample is kept at 4 K in a low-vibration closed-cycle He cryostat *At-tocube - Attody800*. The QD source is pumped with a 79 MHz-pulsed laser shaped with a QShaper (Quandela) 4f pulse shaper to select a specific wavelength and achieve a bandwidth of ~ 100 pm. The optical excitation of the QD is achieved in an LA phonon assisted configuration with a laser at 927.2 nm blue-detuned from the transition [78], which enables single-photon generation by exciton emission at (927.8 ± 0.2) nm (Fig. 2-a). The emitted photons are directly coupled in single-mode fiber (SMF) and spectrally separated from the residual pumping laser with bandpass filters. At the output of the *e-Delight-LA* system, we measure a single-photon count rate of $R_{\text{det}} = 4$ MHz. The fibered brightness of the single-photon source depends mainly on the coupling efficiency into the SMF, the spectral separation transmission of the single-photon stream from the pump laser - whose effects we estimate in an overall efficiency of $\eta_{\text{setup}} \sim 52\%$ - and the detector efficiency, estimated to be around $\eta_{\text{det}} \sim 38\%$. Using this figures, we estimate a *first lens brightness* of $B = \frac{R_{\text{det}}}{R_{\text{exc}} \eta_{\text{det}} \eta_{\text{setup}}} \sim 26\%$, where R_{exc} is the pump frequency. The overall quality of the single-photon generation can be characterized by measuring the multi-photon emission and indistinguishability. Using a standard Hanbury Brown and Twiss setup, we measured an second-order auto-correlation of $g^{(2)}(0) = (1.26 \pm 0.05)\%$. Such figure is computed by normalizing the zero-time delay coincidences to the side peaks coincidences between two consecutive near-resonant excitations (Fig. 2-b). We also measured the indistinguishability between photons successively emitted by the QD, through a Hong-Ou-Mandel (HOM) interference experiment [79]. Two consecutively emitted photons are split by a beam splitter (BS) and coupled in SMFs, whose length is chosen to delay one of them by ≈ 12.5 ns to ensure temporal overlap on a second BS. At its outputs, photons are collected in Avalanche Photodiode Detectors (APDs) to record photons coincidence counts. Therefore, we evaluate a 2-photon interference visibility derived from the correlation histogram (Fig. 2-c) as $V_{HOM} = 1 - 2 \frac{C_0}{\langle C \rangle_{t \rightarrow \infty}}$, where C_0 are the counts when the two photons are synchronized and $\langle C \rangle_{t \rightarrow \infty}$ are the average peak counts for relative temporal delays larger than one repetition rate of the laser. We measure an interference visibility $V_{HOM} = (93.05 \pm 0.06)\%$, which can be corrected to account for unwanted multi-photon components [77], resulting in a photon indistinguishability equal to $M_s = (95.5 \pm 0.1)\%$.

B. Experimental implementation of OAM-based platform

We experimentally implemented a flexible platform for the study of single and multi-photons properties, and capable of implementing a probabilistic entangling quantum gate. A visual scheme of the setup is reported in Fig. 3.

For this purpose, the stream of single photons generated by the QD is preliminarily split through a fiber-BS and OAM encoding is performed separately on the two outputs. In particular, the input state, $|H, 0\rangle$, having horizontal polarization and null OAM value, is selected through single mode fibers and polarizing beam splitters (PBS). In the engineering stage,

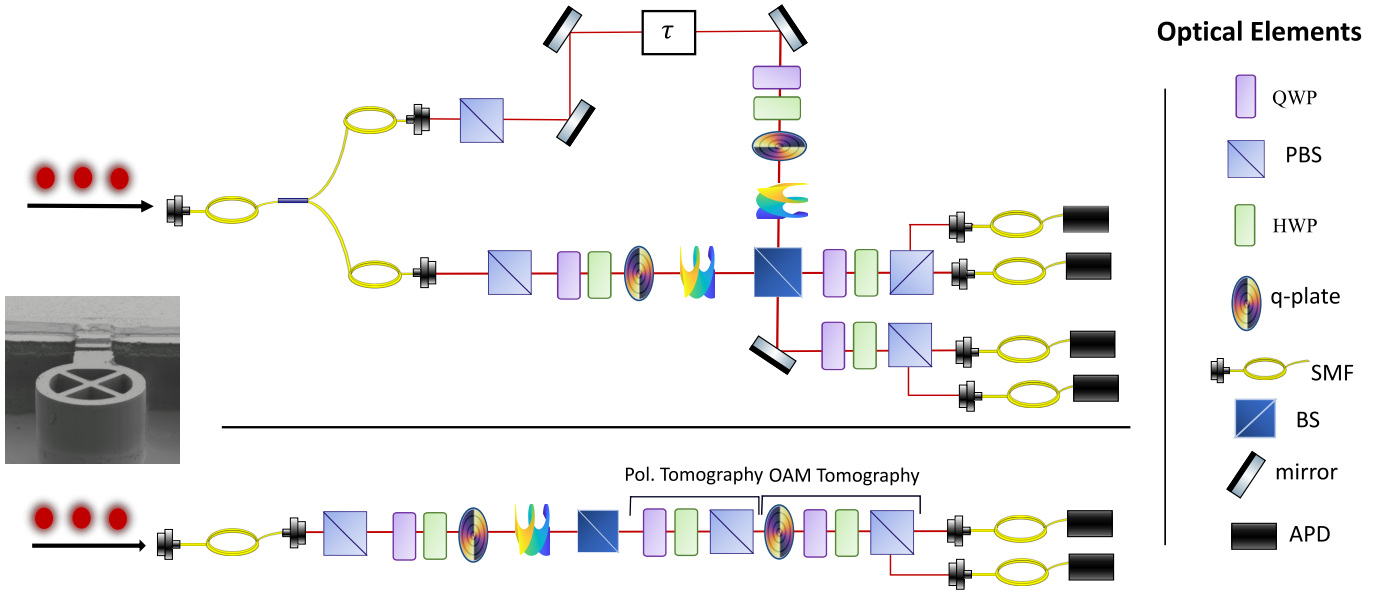


Figure 3. **Experimental Setup.** Single-photon states at a wavelength of 927.8 ± 0.2 nm are generated using a QD source pumped with a shaped 79 MHz-pulsed laser at 927.2 nm. Then a fiber-BS splits the photons between the two arms of the setup, and after passing through a PBS the input states have horizontal polarization and OAM eigenvalue $m = 0$. In both paths, series of QWP, HWP and q-plate are used to produce OAM modes of the form reported in Eq. (2), while in one of the arms, a delay line (τ) is inserted in order to synchronize on the BS the photons emitted in different pulses of the pump beam. The *intra*-particle regime is investigated removing the fiber-BS and performing all the experiment on a single line, involving the first input and output of the BS, as shown in the below panel. On the other hand, in the *inter*-particle experiment, the photons are sent to the fiber-BS and the gate is implemented interfering on the second BS. After passing through the BS the state of the photons is analyzed, coupled to SMFs and detected by APDs. The measurement setup consists in two different stages, a series of q-plate, QWP, HWP and PBS is used to study the OAM states of the photons coupled with the polarization, while a QWP, HWP and a PBS compose the polarization analysis setup. In the *inter*-particle regime only OAM analysis is performed on the photon pairs. While, in the *intra*-particle regime both analysis setups are used to separately investigate the polarization and OAM content of single photons, as shown in the below panel.

by placing a set of waveplates together with a q-plate on each arm, we are able to independently generate two distinct OAM-encoded single-photon states. In particular, a q-plate is a thin film of birefringent material (in our case, nematic liquid crystals) characterized by a non-uniform distribution of the optic axis across the plane transverse to the light propagation direction. The angle between the optic axis and the horizontal axis x of the device follows the relation $\alpha(\phi) = \alpha_0 + q\phi$, where ϕ is the azimuthal angle in the transverse plane, α_0 is the optic axis orientation for $\phi = 0$ and q is the topological charge, i.e. the winding number of the optic axis for $\phi \in [0, 2\pi]$. Owing to the inhomogeneity of its optic axis distribution and to the resulting Pancharatnam-Berry geometric phases, the q-plate develops on the OAM degree of freedom of single photons an action that depends on their polarization, according to the following expression [58, 59]:

$$\hat{Q} = \sum_m |m-2q\rangle \langle m| \otimes |L\rangle \langle R| + |m+2q\rangle \langle m| \otimes |R\rangle \langle L|, \quad (1)$$

where $|R\rangle, |L\rangle$ indicate respectively right and left circular polarization states and $|m\rangle$ represents the OAM value.

Therefore, an optical setup consisting of a quarter-waveplate (QWP), a half-waveplate (HWP) and a q-plate with $q = 1$, acting on the input state $|H, 0\rangle$, is able to engineer arbitrary superpositions of $|L, -2\rangle$ and $|R, 2\rangle$ as given by:

$$|\Phi\rangle = \cos(\theta/2) |L, -2\rangle + e^{i\psi} \sin(\theta/2) |R, 2\rangle \quad (2)$$

where, $\theta \in [0, \pi]$ and $\psi \in [0, 2\pi]$ can be set by properly orienting the optic axes of QWP and HWP. In this way, *intra*-system entanglement between OAM and SAM degrees of freedom of single photons can be easily achieved. In particular, for $\theta = \pi/2$, the superpositions given in Eq. (2) correspond to the above mentioned VV states.

Subsequently, the two arms are synchronized by introducing a fixed delay in fiber and a tunable delay in air and then sent to a bulk beam splitter (BS) used to probabilistically generate an entangled state between the two photons in the hybrid space of OAM and SAM by a postselection on the measured events.

Finally, in both *intra*- and *inter*- experiment the state reconstruction is performed by using q-plates and polarization tomography setups comprising a QWP and a HWP followed by a PBS. In fact, the OAM tomography setup is implemented by adding a q-plate in front of the polarization tomography setup to convert the correlations present in the OAM degree of freedom on the polarization space, as can be evinced from Eq. (1). In particular, in the *intra*-particle regime, the fiber-BS is removed and the entangled state is generated along the lower arm of the interferometer. Both the polarization and OAM analysis of such states is performed along one BS output, by inserting the polarization tomography setups followed by the OAM tomography one. Instead, the analysis of the *inter*-particle entangled state is performed by placing only the OAM tomography setups on each BS output. After the projection,

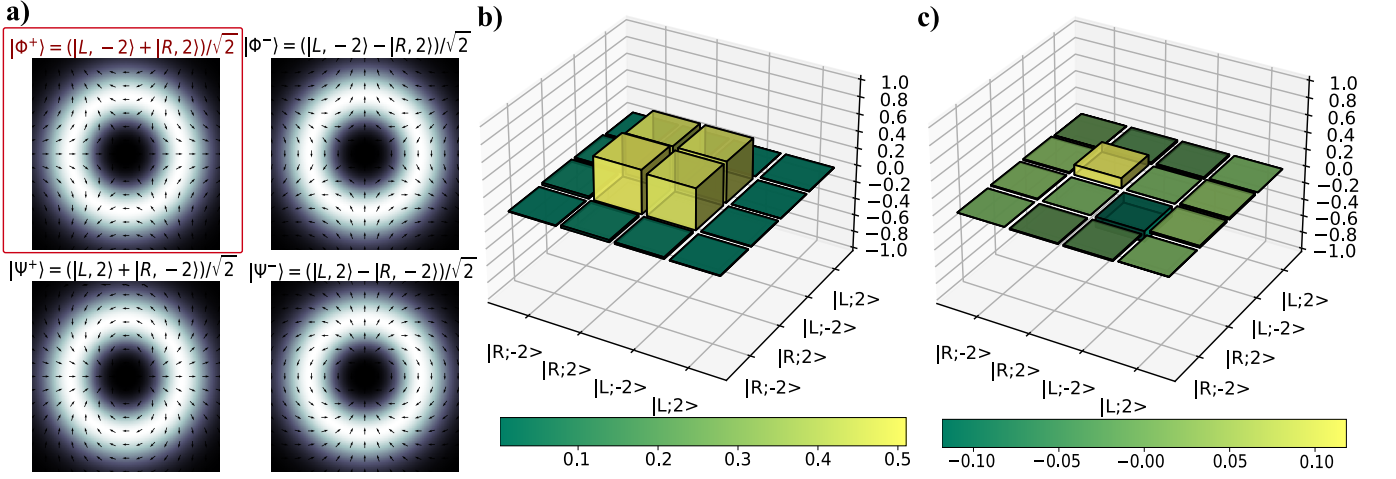


Figure 4. **Intra-particle entangled state:** (a) Intensity and polarization patterns of the Bell states basis in the combined OAM and polarization space. As highlighted by the red box, we focused our attention on the $|\Phi^+\rangle$ state. (b) Real and (c) imaginary parts of the measured density matrix for the $|\Phi^+\rangle$ state reconstructed via quantum state tomography. The fidelity between the reconstructed state and the theoretical one is equal to $\mathcal{F} = 0.9714 \pm 0.0007$, where the standard deviations are estimated through a Monte Carlo approach assuming a Poissonian statistics.

the photons are collected in SMFs and detected using APDs. This scheme is used both to study the entanglement content of the states through Bell inequalities violation and to perform quantum state tomographies.

III. ENTANGLEMENT CERTIFICATION

In this section, we provide the theoretical description and report the results obtained studying the *intra*-particle and *inter*-particle hybrid entanglement generated with the experimentally implemented platform. In all cases of interest, entanglement is certified through a violation of a CHSH Bell inequality and complete state tomography.

A. Vector vortex beam: *intra*-system entanglement

The first investigation regards the generation of VV beams encoded into the single-photon states generated by the QD source. The VV beams are superpositions of two or more different OAM beams associated to orthogonal circular polarizations, an example is given in Eq. (2). Here, the two systems individuated by the OAM eigenstates $\{|-2\rangle, |2\rangle\}$ and the polarization states $\{|R\rangle, |L\rangle\}$ can be exploited for encoding two qubits. In this way, it is possible to define a complete basis of maximally entangled states between these two degrees of freedom. The set of Bell-like states is reported in Fig.4, in which the non-uniform polarization distribution in the transverse plane is highlighted.

In our setup, to increase the generation rate, the signal is sent only in one of the two arms of the interferometer by removing the first fiber-BS (see Fig.3). The VV beams are prepared by making horizontally polarized photons passing subsequently through a QWP, a HWP and a q-plate with $q = 1$. In this way, the state produced by the device is described by $\theta = \pi/2$ in Eq.

(2) and a value of ψ which depends on the α_0 of the q-plate optic axis. This additional phase term is compensated by a further HWP (not shown in Fig. 3) in order to have $\psi = 0$. The final entangled state between OAM and polarization will be

$$|\Phi^+\rangle = \frac{1}{\sqrt{2}} [|L, -2\rangle + |R, 2\rangle] \quad (3)$$

Although such entanglement structure is not associated with non-local properties since it is encoded in a single carrier, these correlations can be detected using Bell-like inequalities. We refer to such type of quantum correlations as *intra*-particle entanglement.

The adoption of a nearly-deterministic single-photon source allows us to perform the *intra*-particle analysis without the need of heralding measurements or post-selection. The latter are unavoidable procedures for generating single-photon states with high purity via probabilistic sources. This reduces drastically the losses allowing to reach a rate of $\simeq 99$ kHz of VV states generation (see Supplemental Information for further details). The quality of the state and of its entanglement structure has been certified by the measurement stage setup shown and described in Section II. In particular, we performed a quantum state tomography by analysing the OAM and the polarization independently via cascaded measurement stages as in the below panel of Fig. 3. The resulting density matrix is reported in Fig. 4 and the relative fidelity, computed by subtracting for dark counts, is $\mathcal{F} = 0.9714 \pm 0.0007$. Moreover, we also certified the *intra*-particle entanglement by evaluating a CHSH-like inequality. Collecting data for 20 s, we obtained a raw violation of $S^{(raw)} = 2.736 \pm 0.008$ which exceeds the separable bound by 92 standard deviations, while the value obtained by subtracting the background signal is $S = 2.792 \pm 0.008$ which exceeds the classical bound by 99 standard deviations. The results are summarized in table I.

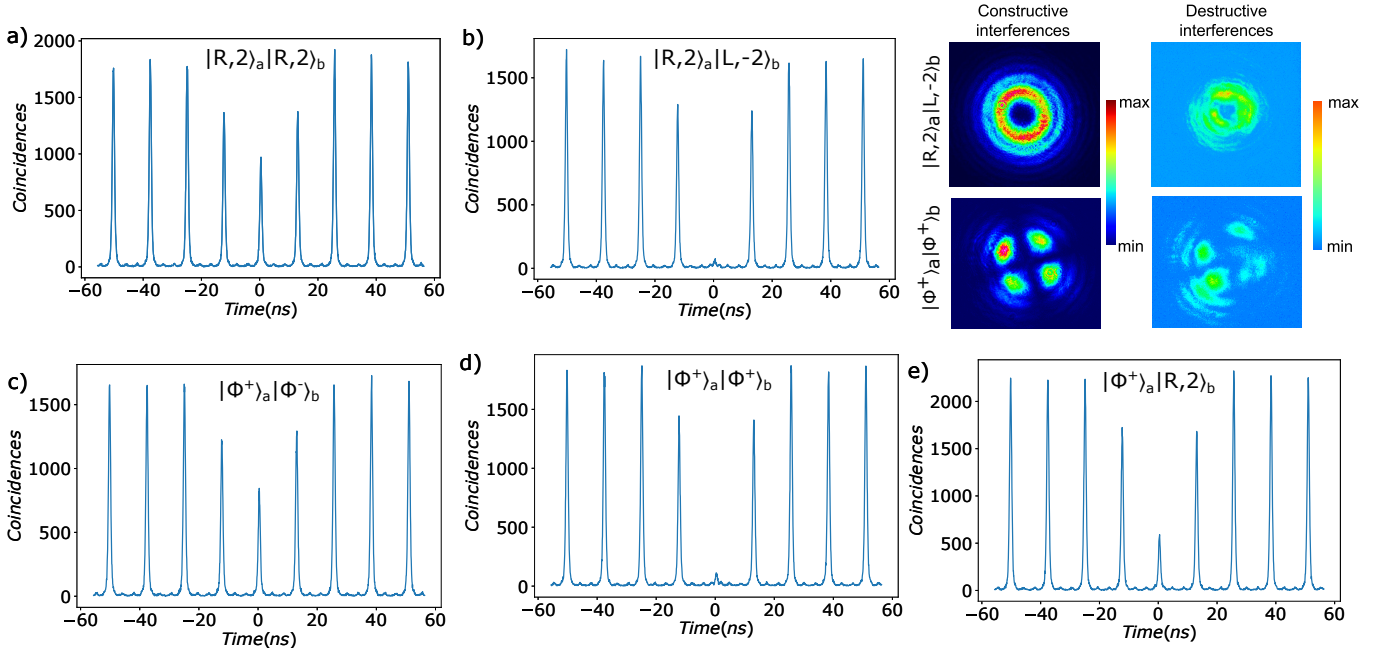


Figure 5. **Hong-Ou-Mandel interference for OAM states:** Measured coincidences at the output of the final BS, see Fig. 3, for different input states in the hybrid space of OAM and polarization. A perfect HOM interference can be obtained only when the photon states are indistinguishable from the point of view of the observer. By knowing the BS action on circular polarization and OAM (see Supplementary Information), we observe a near-unitary visibility when the photons are prepared in the same eigenstate of the BS reflection operation, or when the initial states have opposite circular polarization and OAM value. Moreover, we also analyze the hybrid configuration in which one photon is prepared in the state $|R, 2\rangle$ and the other in the VV state $|\Phi^+\rangle$. In the latter case, the expected number of coincidences is half of the one obtained for distinguishable photons. In the inset, the intensity patterns associated to constructive and destructive interference are reported for both initial states $|R, 2\rangle_a |L, -2\rangle_b$ and $|\Phi^+\rangle_a |\Phi^+\rangle_b$.

B. Certification of photon states generation

In quantum information processes, an important computational resource relies on the capability of manipulating multiple photons and making them interact. Therefore, in this section, we assess the capacity of codifying specific OAM states on photons generated by subsequent pulsed pumping of the QD. This is performed by evaluating the visibility of HOM interference in a beam-splitter which is equivalent to a pairwise overlap estimation in a SWAP test [80]. There are some previous examples of HOM experiments with single-photon states carrying OAM [38, 81], but our tests are among the first to be applied to vector beams generated by a deterministic single-photon source.

Let us first briefly review the effect of an unbiased BS on the field annihilation and creation operators, \hat{a}, \hat{a}^\dagger and \hat{b}, \hat{b}^\dagger . The relation between input modes $\{a, b\}$ and output modes $\{c, d\}$ can be expressed as (Fig. 2):

$$\begin{aligned}\hat{a}^\dagger &\mapsto \frac{1}{\sqrt{2}} (\hat{c}^\dagger - \hat{d}^\dagger) \\ \hat{b}^\dagger &\mapsto \frac{1}{\sqrt{2}} (\hat{c}^\dagger + \hat{d}^\dagger).\end{aligned}\quad (4)$$

By considering two photons at the two inputs of the beam splitter, the signature of the interference is a change in the probability to detect photons in different outputs (see Supplementary Information). In particular, two photons are indistinguishable

if their states, associated to each degree of freedom, is the same from the point of view of the observer. To approach this condition in our setup, a delay line is used to synchronize the photons in the temporal domain. This is mandatory because the two single photons are emitted by the QD at different times. However, when the photons are characterized by OAM value different from zero and superposed polarizations, it is necessary to take into account the effect of reflections. Indeed, in a physical beam-splitter the semi-reflective mirror flips the elicity of both OAM and polarization. In other words, after one reflection we have $\{|R\rangle, |L\rangle\} \rightarrow \{|L\rangle, |R\rangle\}$ and $|\pm 2\rangle \rightarrow |\mp 2\rangle$, while horizontal and vertical polarizations are eigenstates of this operation with eigenvalues of opposite signs. Then, we have that the creation operators are changed as follows:

$$\begin{aligned}\hat{a}_R^\dagger, \hat{b}_R^\dagger &\mapsto \frac{1}{\sqrt{2}} (\hat{c}_R^\dagger - \hat{d}_L^\dagger), \quad \frac{1}{\sqrt{2}} (\hat{c}_L^\dagger + \hat{d}_R^\dagger) \\ \hat{a}_L^\dagger, \hat{b}_L^\dagger &\mapsto \frac{1}{\sqrt{2}} (\hat{c}_L^\dagger - \hat{d}_R^\dagger), \quad \frac{1}{\sqrt{2}} (\hat{c}_R^\dagger + \hat{d}_L^\dagger) \\ \hat{a}_m^\dagger, \hat{b}_m^\dagger &\mapsto \frac{1}{\sqrt{2}} (\hat{c}_m^\dagger - \hat{d}_{-m}^\dagger), \quad \frac{1}{\sqrt{2}} (\hat{c}_{-m}^\dagger + \hat{d}_m^\dagger).\end{aligned}\quad (5)$$

Since the indistinguishability of photons generated by the source has been already checked in Section II A, here we are interested in computing the overlap between VV states encoded in different photons. As for the previous analysis, the OAM and polarization degrees of freedom are controlled through a series of QWP, HWP and q-plate placed in each arm of the

interferometer. This allows us to prepare the desired state for each photon.

Considering the BS action in Eq. (5), we expect no interference when the two photons are prepared as $|R, 2\rangle_a |R, 2\rangle_b$, since the reflected beam and the transmitted one in the outputs c and d will display orthogonal states. Conversely, the HOM effect occurs when the initial state is $|R, 2\rangle_a |L, -2\rangle_b$. The correlation histograms, obtained via a HOM interference experiment, for both input states $|R, 2\rangle_a |R, 2\rangle_b$ and $|R, 2\rangle_a |L, -2\rangle_b$ are reported in Fig. 5-a,b. The visibility of such HOM experiments quantifies the variation, from the maximum to minimum overlapping between the wavefunctions, of the probability to detect photons in different outputs. The obtained visibilities are $V_{|R,2\rangle,|R,2\rangle} = -4 \pm 1\%$ and $V_{|R,2\rangle,|L,-2\rangle} = 90.1 \pm 0.3\%$, respectively.

We repeat the same interference scheme with VV states such as $|\Phi^+\rangle$ and $|\Phi^-\rangle$ (see Fig. 4). For these classes of states we note that they are symmetric with respect to the BS operation. This means that the reflected photon and the transmitted one always display the same state if they are indistinguishable at the input faces of the beam-splitter (see Supplementary information). The resulting HOM correlations for the input state $|\Phi^+\rangle_a |\Phi^-\rangle_b$ are reported in Fig. 5-c and the achieved visibility is equal to $V_{|\Phi^+,\Phi^-} = 0.70 \pm 0.10\%$, as expected. On the contrary, when the two photons are prepared in the same VV states such as $|\Phi^+\rangle_a |\Phi^+\rangle_b$, the theoretical HOM visibility is 1. We measured $V_{|\Phi^+,\Phi^+} = 88.2 \pm 0.3\%$, as reported in Fig. 5-d.

A further peculiar configuration is when the interfering input states are neither equal nor orthogonal, for which we expect a $V = \frac{1}{2}$. This is the case of two photons prepared in the input ports as $|\Phi^+\rangle_a |R, 2\rangle_b$. The measured visibility is $V_{|\Phi^+,\text{R},2} = 44.5 \pm 0.6\%$ (Fig. 5-e).

C. 2-photons quantum gate: *inter*-system entanglement

The configuration described in the previous section can be exploited to implement a multi-qubit probabilistic quantum gate able to generate an entangled state in the hybrid space composed by OAM and polarization. In particular, by post-selecting on the two-photon coincidence events resulting from the preparation $|R, 2\rangle_a |R, 2\rangle_b$, and noticing that one of the output is affected by a further reflection which introduces a phase π between horizontal and vertical polarization, and inverts the OAM value, the following maximally entangled state is generated:

$$\begin{aligned} |\Phi\rangle &= \frac{|L, -2\rangle_c |R, 2\rangle_d + |R, 2\rangle_c |L, -2\rangle_d}{\sqrt{2}} \\ &= \frac{|1, 0\rangle |0, 1\rangle + |0, 1\rangle |1, 0\rangle}{\sqrt{2}}, \end{aligned} \quad (6)$$

where we took off the direction subscript $\{c, d\}$ and we identified $|L, -2\rangle = |1, 0\rangle$ and $|R, 2\rangle = |0, 1\rangle$. Therefore, the generated state is a maximally entangled state in the 4-dimensional OAM-SAM Hilbert space. However, in the hybrid

OAM-SAM space, this state can be also considered equivalent to a two-dimensional maximally entangled state. Indeed, re-labeling the state $|L, -2\rangle$ as qubit $|0\rangle$ and the state $|R, 2\rangle$ as qubit $|1\rangle$, the state in Eq. (6) results to be equivalent to a triplet Bell state:

$$\begin{aligned} |\Phi\rangle &= \frac{|L, -2\rangle_c |R, 2\rangle_d + |R, 2\rangle_c |L, -2\rangle_d}{\sqrt{2}} = \\ &= \frac{|0\rangle |1\rangle + |1\rangle |0\rangle}{\sqrt{2}} \end{aligned} \quad (7)$$

Therefore, this state exhibit quantum correlations that could be detected by performing a Bell-like test which is used as an entanglement witness. In particular, we evaluated a CHSH-like inequality performing the projective measurements placing the OAM measurement stage, reported in Fig. 3, on both BS outputs. Collecting data for 400 s and with a coincidence rate of 146 Hz, we obtained a raw violation of $S^{(raw)} = 2.516 \pm 0.006$ which exceeds the classical bound by 86 standard deviations, while the value obtained by subtracting the accidental coincidences is $S = 2.779 \pm 0.006$ which exceeds the separable bound by 130 standard deviations.

Moreover, we also performed a complete quantum state tomography of the state using the same experimental configuration. The retrieved density matrix is shown in Fig. 6, analyzing the fidelity with the triplet Bell state, we obtained a value of $\mathcal{F} = 0.935 \pm 0.002$ by subtracting for accidental coincidences. The results are summarized in table I. It is worth noting that the decrease in the coincidence rate is mainly due to the coupling efficiency into SMFs in the detection stage of about 45% (see Supplementary Information for further details). This lower value depends on both the limited conversion efficiency of the QPs and on the higher divergence to which beams endowed with orbital angular momentum are subjected. Looking toward gates with more than two photons, the rate could be improved by compensating for losses due to the divergence.

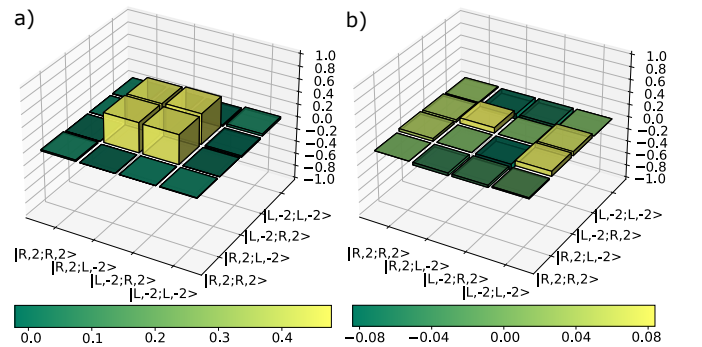


Figure 6. **Inter-particle entangled state:** Real (a) and imaginary (b) parts of the measured density matrix for the two photons state in the hybrid OAM-polarization space reported in Eq. (7), these are reconstructed via quantum state tomography. The fidelity between the reconstructed state and the theoretical one is equal to $\mathcal{F} = 0.935 \pm 0.002$, where the standard deviation are estimated through a Monte Carlo approach assuming a Poissonian statistics.

State	T (s)	Rate (Hz)	$S^{(raw)}$	S	\mathcal{F}
Intra	20	99000	2.736(8)	2.792(8)	0.9714(7)
Inter	400	146	2.516(6)	2.779(6)	0.935(2)

Table I. **Experimental Results:** The table shows the results obtained both for the *intra*-particle and *inter*-particle regime. Here are reported the measurement acquisition time T, the generation rate and the values for the Bell parameter (S) and the fidelity. In particular, the violation $S^{(raw)}$ is computed using raw data, while the parameter S is obtained subtracting the background signal or the accidental coincidence, respectively. The fidelity value is computed comparing the reconstructed density matrix with the triplet Bell state.

IV. CONCLUSIONS

In this paper, we experimentally implemented a platform capable of generating on demand photonic quantum states in high-dimensional Hilbert spaces. This was achieved by combining a bright QD source with q-plates, devices capable of coupling OAM and polarization of single photons, placed in an interferometric configuration. After assessing the properties of the source, such as the multiphoton component, and the indistinguishability of the emitted photons, we focused on the generation and analysis of entangled states in the hybrid space composed of orbital angular momentum and polarization. The setup allows us to study both the *intra*- and *inter*-particle entanglement. For the former, we generated a VV state using only the engineering stage placed in one arm of the interferometer, while for the latter we exploited the interference between modulated single photons generated by the QD in two consecutive excitations to implement a probabilistic quantum gate capable

of producing entangled two-photon states. The characterization of the interferometer scheme was preliminarily performed by evaluating the overlap between quantum states of single photons encoded in the hybrid Hilbert space. In particular, we observed high HOM visibilities for single photons that turn out to be indistinguishable in the detection stage, while very low visibility was observed for orthogonal quantum states. The qualities of both *intra*- and *inter*- particle hybrid entangled states were evaluated by performing quantum state tomography and by using Bell tests to estimate the CHSH inequality. The high values of fidelities and inequality violations highlights the performances of the proposed setup for the engineering of high-dimensional entangled states.

In summary, we proposed and implemented experimentally a flexible platform able to generate both nearly-deterministic single-photon states that exhibit entanglement between OAM and SAM degrees of freedom, and two-photon entangled states in an Hilbert space with dimensions up to four. The employed simple and effective scheme could be extended to the multiphoton regime, opening the way to high-dimensional multiphoton experiments, whose scalability is extremely demanding for platforms based on probabilistic sources. In conclusion, the results demonstrated in the present manuscript can provide advances both for fundamental investigations and quantum photonic applications.

ACKNOWLEDGEMENTS

This work is supported by the European Union's Horizon 2020 research and innovation programme under the PHOQU-SING project GA no. 899544, by the European Union's Horizon 2020 Research and Innovation Programme QUDOT-TECH under the Marie Skłodowska-Curie Grant Agreement No. 86109.

-
- [1] H. Rubinsztein-Dunlop, A. Forbes, M. V. Berry, M. R. Dennis, D. L. Andrews, M. Mansuripur, C. Denz, C. Alpmann, P. Banzer, T. Bauer, and et al., *Journal of Optics* **19**, 013001 (2016).
 - [2] L. Allen, M. W. Beijersbergen, R. J. C. Spreeuw, and J. P. Woerdman, *Phys. Rev. A* **45**, 8185 (1992).
 - [3] M. P. Lavery, F. C. Speirits, S. M. Barnett, and M. J. Padgett, *Science* **341**, 537 (2013).
 - [4] L. Torner, J. P. Torres, and S. Carrasco, *Opt. Express* **13**, 873 (2005).
 - [5] D. S. Simon and A. V. Sergienko, *Phys. Rev. A* **85**, 043825 (2012).
 - [6] N. Uribe-Patarroyo, A. Fraine, D. S. Simon, O. Minaeva, and A. V. Sergienko, *Phys. Rev. Lett.* **110**, 043601 (2013).
 - [7] Q. Zhan, *Optics express* **12**, 3377 (2004).
 - [8] A. E. Willner, H. Huang, Y. Yan, Y. Ren, N. Ahmed, G. Xie, C. Bao, L. Li, Y. Cao, Z. Zhao, and et al., *Advances in Optics and Photonics* **7**, 66 (2015).
 - [9] M. Malik, M. O'Sullivan, B. Rodenburg, M. Mirhosseini, J. Leach, M. P. Lavery, M. J. Padgett, and R. W. Boyd, *Optics express* **20**, 13195 (2012).
 - [10] J. Wang, J.-Y. Yang, I. M. Fazal, N. Ahmed, Y. Yan, H. Huang, Y. Ren, Y. Yue, S. Dolinar, M. Tur, and et al., *Nature Photonics* **6**, 488–496 (2012).
 - [11] J. Baghdady, K. Miller, K. Morgan, M. Byrd, S. Osler, R. Ragusa, W. Li, B. M. Cochenour, and E. G. Johnson, *Optics express* **24**, 9794 (2016).
 - [12] N. Bozinovic, Y. Yue, Y. Ren, M. Tur, P. Kristensen, H. Huang, A. E. Willner, and S. Ramachandran, *Science* **340**, 1545–1548 (2013).
 - [13] G. Gibson, J. Courtial, M. J. Padgett, M. Vasnetsov, V. Pas'ko, S. M. Barnett, and S. Franke-Arnold, *Optics express* **12**, 5448 (2004).
 - [14] M. Krenn, J. Handsteiner, M. Fink, R. Fickler, R. Ursin, M. Malik, and A. Zeilinger, *Proc. Nat. Acad. Sci. USA* **29**, 13648 (2016).
 - [15] D. Cozzolino, B. Da Lio, D. Bacco, and L. K. Oxenløwe, *Advanced Quantum Technologies* **2**, 1900038 (2019).
 - [16] M. Krenn, J. Handsteiner, M. Fink, R. Fickler, and A. Zeilinger, *Proceedings of the National Academy of Sciences* **112**, 14197 (2015).

- [17] M. Malik, M. Erhard, M. Huber, M. Krenn, R. Fickler, and A. Zeilinger, *Nature Photonics* **10**, 248 (2016).
- [18] D. Cozzolino, E. Polino, M. Valeri, G. Carvacho, D. Bacco, N. Spagnolo, L. K. Oxenløwe, and F. Sciarrino, *Advanced Photonics* **1**, 046005 (2019).
- [19] Y. Zhou, M. Mirhosseini, S. Oliver, J. Zhao, S. M. H. Rafsanjani, M. P. Lavery, A. E. Willner, and R. W. Boyd, *Optics express* **27**, 10383 (2019).
- [20] X.-L. Wang, X.-D. Cai, Z.-E. Su, M.-C. Chen, D. Wu, L. Li, N.-L. Liu, C.-Y. Lu, and J.-W. Pan, *Nature* **518**, 516 (2015).
- [21] M. Mirhosseini, O. S. Magaña-Loaiza, M. N. O’Sullivan, B. Rodenburg, M. Malik, M. P. J. Lavery, M. J. Padgett, D. J. Gauthier, and R. W. Boyd, *New Journal of Physics* **17**, 033033 (2015).
- [22] A. Sit, F. Bouchard, R. Fickler, J. Gagnon-Bischoff, H. Larocque, K. Heshami, D. Elser, C. Peuntinger, K. Günthner, B. Heim, C. Marquardt, G. Leuchs, R. W. Boyd, and E. Karimi, *Optica* **4**, 1006 (2017).
- [23] F. Bouchard, A. Sit, F. Hufnagel, A. Abbas, Y. Zhang, K. Heshami, R. Fickler, C. Marquardt, G. Leuchs, R. W. Boyd, and E. Karimi, *Optics express* **26**, 22563 (2018).
- [24] F. Cardano, M. Maffei, F. Massa, B. Piccirillo, C. de Lisio, G. D. Filippis, V. Cataudella, E. Santamato, and L. Marrucci, *Nat. Comm.* **7**, 11439 (2016).
- [25] F. Cardano, A. D’Errico, A. Dauphin, M. Maffei, B. Piccirillo, C. de Lisio, G. D. Filippis, V. Cataudella, E. Santamato, L. Marrucci, M. Lewenstein, and P. Massignan, *Nat. Comm.* **8**, 15516 (2017).
- [26] I. Buluta and F. Nori, *Science* **326**, 108 (2009).
- [27] B. P. Lanyon, M. Barbieri, M. P. Almeida, T. Jennewein, T. C. Ralph, K. J. Resch, G. J. Pryde, J. L. O’Brien, A. Gilchrist, and A. G. White, *Nature Physics* **5**, 134 (2009).
- [28] T. C. Ralph, K. J. Resch, and A. Gilchrist, *Phys. Rev. A* **75**, 022313 (2007).
- [29] B. Hiesmayr, M. De Dood, and W. Löffler, *Physical review letters* **116**, 073601 (2016).
- [30] H. Bechmann-Pasquinucci and A. Peres, *Phys. Rev. Lett.* **85**, 3313 (2000).
- [31] L. Sheridan and V. Scarani, *Physical Review A* **82**, 030301 (2010).
- [32] M. Li, S. Yan, Y. Liang, P. Zhang, and B. Yao, *Physical Review A* **95**, 053802 (2017).
- [33] F. Cardano and L. Marrucci, *Nature Photonics* **9**, 776 (2015).
- [34] G. Vallone, V. D’Ambrosio, A. Sponselli, S. Slussarenko, L. Marrucci, F. Sciarrino, and P. Villoresi, *Phys. Rev. Lett.* **113**, 060503 (2014).
- [35] V. D’Ambrosio, E. Nagali, S. P. Walborn, L. Aolita, S. Slussarenko, L. Marrucci, and F. Sciarrino, *Nature Communications* **3** (2012).
- [36] S. Slussarenko, E. Karimi, B. Piccirillo, L. Marrucci, and E. Santamato, *Phys. Rev. A* **80**, 022326 (2009).
- [37] E. Nagali, F. Sciarrino, F. D. Martini, B. Piccirillo, E. Karimi, L. Marrucci, and E. Santamato, *Opt. Express* **17**, 18745 (2009).
- [38] E. Nagali, L. Sansoni, F. Sciarrino, F. De Martini, L. Marrucci, B. Piccirillo, E. Karimi, and E. Santamato, *Nature Photonics* **3**, 720 (2009).
- [39] L.-P. Deng, H. Wang, and K. Wang, *J. Opt. Soc. Am. B* **24**, 2517 (2007).
- [40] Y. Chen, J. Gao, Z.-Q. Jiao, K. Sun, W.-G. Shen, L.-F. Qiao, H. Tang, X.-F. Lin, and X.-M. Jin, *Physical Review Letters* **121**, 233602 (2018).
- [41] B. P. da Silva, M. A. Leal, C. E. R. Souza, E. F. Galvão, and A. Z. Khoury, *Journal of Physics B: Atomic, Molecular and Optical Physics* **49**, 055501 (2016).
- [42] V. Parigi, V. D’Ambrosio, C. Arnold, L. Marrucci, F. Sciarrino, and J. Laurat, *Nature communications* **6**, 1 (2015).
- [43] T. Giordani, A. Suprano, E. Polino, F. Acanfora, L. Innocenti, A. Ferraro, M. Paternostro, N. Spagnolo, and F. Sciarrino, *Phys. Rev. Lett.* **124**, 160401 (2020).
- [44] A. R. C. Pinheiro, C. E. R. Souza, D. P. Caetano, J. A. O. Huguenin, A. G. M. Schmidt, and A. Z. Khoury, *J. Opt. Soc. Am. B* **30**, 3210 (2013).
- [45] Y. Kozawa, D. Matsunaga, and S. Sato, *Optica* **5**, 86 (2018).
- [46] A. Suprano, T. Giordani, I. Gianani, N. Spagnolo, K. Pinker, J. Kupferman, S. Arnon, U. Klemm, D. Gorpas, V. Ntziachristos, *et al.*, *Optics Express* **28**, 35427 (2020).
- [47] E. Polino, M. Valeri, N. Spagnolo, and F. Sciarrino, *AVS Quantum Science* **2**, 024703 (2020).
- [48] R. Fickler, R. Lapkiewicz, W. N. Plick, M. Krenn, C. Schaeff, S. Ramelow, and A. Zeilinger, *Science* **338**, 640 (2012).
- [49] S. Berg-Johansen, F. Töppel, B. Stiller, P. Banzer, M. Ornigotti, E. Giacobino, G. Leuchs, A. Aiello, and C. Marquardt, *Optica* **2**, 864 (2015).
- [50] C. K. Hong, Z. Y. Ou, and L. Mandel, *Phys. Rev. Lett.* **59**, 2044 (1987).
- [51] F. Bouchard, A. Sit, Y. Zhang, R. Fickler, F. M. Miatto, Y. Yao, F. Sciarrino, and E. Karimi, *Reports on Progress in Physics* **84**, 012402 (2020).
- [52] E. Karimi, D. Giovannini, E. Bolduc, N. Bent, F. M. Miatto, M. J. Padgett, and R. W. Boyd, *Phys. Rev. A* **89**, 013829 (2014).
- [53] Y. Zhang, S. Prabhakar, C. Rosales-Guzmán, F. S. Roux, E. Karimi, and A. Forbes, *Phys. Rev. A* **94**, 033855 (2016).
- [54] M. Hiekkämäki and R. Fickler, *Phys. Rev. Lett.* **126**, 123601 (2021).
- [55] B. Chen, Y. Wei, T. Zhao, S. Liu, R. Su, B. Yao, Y. Yu, J. Liu, and X. Wang, *Nature Nanotechnology* **16**, 302 (2021).
- [56] R. Fickler, M. Krenn, R. Lapkiewicz, S. Ramelow, and A. Zeilinger, *Scientific reports* **3**, 1 (2013).
- [57] E. Yao, S. Franke-Arnold, J. Courtial, M. J. Padgett, and S. M. Barnett, *Opt. Express* **14**, 13089 (2006).
- [58] L. Marrucci, C. Manzo, and D. Paparo, *Phys. Rev. Lett.* **96**, 163905 (2006).
- [59] L. Marrucci, E. Karimi, S. Slussarenko, B. Piccirillo, E. Santamato, E. Nagali, and F. Sciarrino, *J. Opt* **13**, 064001 (2011).
- [60] A. Sit, F. Bouchard, R. Fickler, J. Gagnon-Bischoff, H. Larocque, K. Heshami, D. Elser, C. Peuntinger, K. Günthner, B. Heim, *et al.*, *Optica* **4**, 1006 (2017).
- [61] G. Brassard, N. Lütkenhaus, T. Mor, and B. C. Sanders, *Physical review letters* **85**, 1330 (2000).
- [62] N. Somaschi, V. Giesz, L. De Santis, J. Loredó, M. P. Almeida, G. Hornecker, S. L. Portalupi, T. Grange, C. Anton, J. Demory, *et al.*, *Nature Photonics* **10**, 340 (2016).
- [63] H. Wang, Y.-M. He, T.-H. Chung, H. Hu, Y. Yu, S. Chen, X. Ding, M.-C. Chen, J. Qin, X. Yang, *et al.*, *Nature Photonics* **13**, 770 (2019).
- [64] R. Uppu, F. T. Pedersen, Y. Wang, C. T. Olesen, C. Papon, X. Zhou, L. Midolo, S. Scholz, A. D. Wieck, A. Ludwig, *et al.*, *Science advances* **6**, eabc8268 (2020).
- [65] N. Tomm, A. Javadi, N. O. Antoniadis, D. Najer, M. C. Löbl, A. R. Korsch, R. Schott, S. R. Valentin, A. D. Wieck, A. Ludwig, *et al.*, *Nature Nanotechnology* **16**, 399 (2021).
- [66] E. Waks, K. Inoue, C. Santori, D. Fattal, J. Vuckovic, G. S. Solomon, and Y. Yamamoto, *Nature* **420**, 762 (2002).
- [67] R. Collins, P. Clarke, V. Fernández, K. Gordon, M. Makhonin, J. Timpon, A. Tahraoui, M. Hopkinson, A. Fox, M. Skolnick, *et al.*, *Journal of Applied Physics* **107**, 073102 (2010).
- [68] J.-P. Li, J. Qin, A. Chen, Z.-C. Duan, Y. Yu, Y. Huo, S. Höfling, C.-Y. Lu, K. Chen, and J.-W. Pan, *ACS Photonics* **7**, 1603

- (2020).
- [69] D. Istrati, Y. Pilnyak, J. C. Loredó, C. Antón, N. Somaschi, P. Hilaire, H. Ollivier, M. Esmann, L. Cohen, L. Vidro, C. Millet, A. Lemaitre, I. Sagnes, A. Harouri, L. Lanco, P. Senellart, and H. S. Eisenberg, *Nature Communications* **11**, 5501 (2020).
- [70] J.-P. Li, X. Gu, J. Qin, D. Wu, X. You, H. Wang, C. Schneider, S. Höfling, Y.-H. Huo, C.-Y. Lu, N.-L. Liu, L. Li, and J.-W. Pan, *Phys. Rev. Lett.* **126**, 140501 (2021).
- [71] A. Dousse, J. Suffczyński, A. Beveratos, O. Krebs, A. Lemaitre, I. Sagnes, J. Bloch, P. Voisin, and P. Senellart, *Nature* **466**, 217 (2010).
- [72] K. Takemoto, Y. Nambu, T. Miyazawa, Y. Sakuma, T. Yamamoto, S. Yorozu, and Y. Arakawa, *Scientific reports* **5**, 1 (2015).
- [73] T. Giordani, E. Polino, S. Emiliani, A. Suprano, L. Innocenti, H. Majury, L. Marrucci, M. Paternostro, A. Ferraro, N. Spagnolo, and F. Sciarrino, *Phys. Rev. Lett.* **122**, 020503 (2019).
- [74] A. Suprano, D. Zia, E. Polino, T. Giordani, L. Innocenti, A. Ferraro, M. Paternostro, N. Spagnolo, and F. Sciarrino, *Advanced Photonics* **3**, 066002 (2021).
- [75] V. D'Ambrosio, G. Carvacho, F. Graffitti, C. Vitelli, B. Piccirillo, L. Marrucci, and F. Sciarrino, *Phys. Rev. A* **94**, 030304 (2016).
- [76] E. Karimi, J. Leach, S. Slussarenko, B. Piccirillo, L. Marrucci, L. Chen, W. She, S. Franke-Arnold, M. J. Padgett, and E. Santamato, *Phys. Rev. A* **82**, 022115 (2010).
- [77] H. Ollivier, S. Thomas, S. Wein, I. M. de Buy Wenniger, N. Coste, J. Loredó, N. Somaschi, A. Harouri, A. Lemaitre, I. Sagnes, *et al.*, *Physical Review Letters* **126**, 063602 (2021).
- [78] S. E. Thomas, M. Billard, N. Coste, S. C. Wein, Priya, H. Ollivier, O. Krebs, L. Tazaïrt, A. Harouri, A. Lemaitre, I. Sagnes, C. Anton, L. Lanco, N. Somaschi, J. C. Loredó, and P. Senellart, *Phys. Rev. Lett.* **126**, 233601 (2021).
- [79] C.-K. Hong, Z.-Y. Ou, and L. Mandel, *Physical review letters* **59**, 2044 (1987).
- [80] J. C. Garcia-Escartin and P. Chamorro-Posada, *Phys. Rev. A* **87**, 052330 (2013).
- [81] B. Ndagano and A. Forbes, *APL Photonics* **4**, 016103 (2019).

Orbital angular momentum based *intra*- and *inter*- particle entangled states generated via a quantum dot source

Alessia Suprano,¹ Danilo Zia,¹ Mathias Pont,² Taira Giordani,¹ Giovanni Rodari,¹ Mauro Valeri,¹ Bruno Piccirillo,^{3,4} Gonzalo Carvacho,¹ Nicolò Spagnolo,¹ Pascale Senellart,² Lorenzo Marrucci,³ and Fabio Sciarrino^{1,*}

¹*Dipartimento di Fisica, Sapienza Università di Roma, Piazzale Aldo Moro 5, I-00185 Roma, Italy*

²*Centre for Nanosciences and Nanotechnology, CNRS, Université Paris-Saclay, UMR 9001,10 Boulevard Thomas Gobert, 91120, Palaiseau, France*

³*Dipartimento di Fisica "Ettore Pancini", Università Federico II, Complesso Universitario di Monte Sant'Angelo, Via Cintia, 80126 Napoli, Italy*

⁴*INFN – Sezione di Napoli, Via Cintia, 80126 Napoli, Italy*

arXiv:2211.05160v1 [quant-ph] 9 Nov 2022

* fabio.sciarrino@uniroma1.it

Supplementary Note 1. THEORETICAL BACKGROUND

In this section, we provide a theoretical insight about the different HOM interference cases reported in the main text. Recalling that the action of a symmetric Beam Splitter (BS) with input modes $\{a,b\}$ and output modes $\{c,d\}$ can be expressed as:

$$\begin{pmatrix} \hat{a} \\ \hat{b} \end{pmatrix} = \frac{1}{\sqrt{2}} \begin{pmatrix} 1 & 1 \\ 1 & -1 \end{pmatrix} \begin{pmatrix} \hat{c} \\ \hat{d} \end{pmatrix} \quad (1)$$

Therefore, by considering two photons at the two inputs of the beam splitter, the initial state is $\hat{a}^\dagger \hat{b}^\dagger |0,0\rangle$ and the output state results to be:

$$\frac{1}{2} \left(\hat{c}_a^\dagger \hat{c}_b^\dagger + \hat{c}_a^\dagger \hat{d}_b^\dagger - \hat{c}_b^\dagger \hat{d}_a^\dagger - \hat{d}_a^\dagger \hat{d}_b^\dagger \right) |0,0\rangle, \quad (2)$$

where $|0,0\rangle$ refers to the vacuum in the two ports of the BS and the subscripts a and b to the field modes at the inputs. Two photons are indistinguishable if their state, associated to each degree of freedom, is the same from the point of view of the observer. In this case, when the two initial modes a and b are identical, it is not possible for the observer to discriminate which one of the two photons come out from the outputs c or d . In other words, the term $\hat{c}_a^\dagger \hat{d}_b^\dagger - \hat{c}_b^\dagger \hat{d}_a^\dagger$ vanishes.

For what concern the BS action on the polarization and Orbital Angular Momentum (OAM) states, we have that the horizontal and vertical polarizations result to be eigenstates of the BS operation since the reflection introduces a phase $\phi = \pi$ between them. On the other side, in the OAM space, the eigestates are the balanced superpositions $\frac{|m\rangle + |-m\rangle}{\sqrt{2}}$ and $\frac{|m\rangle - |-m\rangle}{\sqrt{2}}$ which are not affected by the elicity filp.

For instance, considering the case in which the waveplates change the input photons polarization to $|R\rangle$ in both of the arms, after passing through the q-plate (see Main Text, Eq. 1), at the exit of the BS we have:

$$\begin{aligned} & \frac{1}{2} (\hat{c}_{L,-2}^\dagger - \hat{d}_{R,2}^\dagger) (\hat{c}_{R,2}^\dagger + \hat{d}_{L,-2}^\dagger) |0,0\rangle_{cd} = \\ & = \frac{1}{2} (|L,-2\rangle_c |R,2\rangle_c + |L,-2\rangle_c |L,-2\rangle_d - \\ & \quad |R,2\rangle_c |R,2\rangle_d - |R,2\rangle_d |L,-2\rangle_d) \end{aligned} \quad (3)$$

In this case is not possible to extinguish the double coincidence terms and to see the HOM interference we need to enter on the q-plates with orthogonal polarization states. For example, with $|R\rangle_a$ and $|L\rangle_b$ we have:

$$\begin{aligned} & \frac{1}{2} (\hat{c}_{L,-2}^\dagger - \hat{d}_{R,2}^\dagger) (\hat{c}_{L,-2}^\dagger + \hat{d}_{R,2}^\dagger) |0,0\rangle_{cd} = \\ & = \frac{1}{\sqrt{2}} (|L,-2\rangle_c |L,-2\rangle_c - |R,2\rangle_d |R,2\rangle_d) \end{aligned} \quad (4)$$

This behaviour is experimentally observed in our setup as reported in Fig. 5 (a,b) of the Main Text. If instead we enter the q-plates with linearly polarized photons on both the arms, at the output of the BS we observed the complementary behavior in which we observed coincidences only when the photons have orthogonal polarization. In fact considering the input states $|H\rangle_a |H\rangle_b$ and $|H\rangle_a |V\rangle_b$, after the q-plates we have $|\Phi^+\rangle_a |\Phi^+\rangle_b$ and $|\Phi^+\rangle_a |\Phi^-\rangle_b$, then the BS output is respectively:

$$\begin{aligned} a_{\Phi^+}^\dagger b_{\Phi^+}^\dagger & \mapsto \frac{1}{4} (\hat{c}_{R,2}^\dagger - \hat{d}_{L,-2}^\dagger + \hat{c}_{L,-2}^\dagger - \hat{d}_{R,2}^\dagger) (\hat{c}_{L,-2}^\dagger + \hat{d}_{R,2}^\dagger + \hat{c}_{R,2}^\dagger + \hat{d}_{L,-2}^\dagger) |0,0\rangle_{cd} = \\ & = \frac{1}{4} (\sqrt{2} |L,-2\rangle_c |L,-2\rangle_c + \sqrt{2} |R,2\rangle_c |R,2\rangle_c + 2 |L,-2\rangle_c |R,2\rangle_c + \\ & \quad - \sqrt{2} |L,-2\rangle_d |L,-2\rangle_d - 2 |L,-2\rangle_d |R,2\rangle_d - \sqrt{2} |R,2\rangle_d |R,2\rangle_d) \end{aligned} \quad (5)$$

$$\begin{aligned}
a_{\Phi^+}^\dagger b_{\Phi^-}^\dagger &\mapsto \frac{1}{4}(\hat{c}_{R,2}^\dagger - \hat{d}_{L,-2}^\dagger + \hat{c}_{L,-2}^\dagger - \hat{d}_{R,2}^\dagger)(\hat{c}_{L,-2}^\dagger + \hat{d}_{R,2}^\dagger - \hat{c}_{R,2}^\dagger - \hat{d}_{L,-2}^\dagger)|0,0\rangle_{cd} = \\
&= \frac{1}{4}(\sqrt{2}|L,-2\rangle_c |L,-2\rangle_c - \sqrt{2}|R,2\rangle_c |R,2\rangle_c + 2|L,-2\rangle_c |L,-2\rangle_d + \\
&\quad + \sqrt{2}|L,-2\rangle_d |L,-2\rangle_d + 2|R,2\rangle_c |R,2\rangle_d - \sqrt{2}|R,2\rangle_d |R,2\rangle_d)
\end{aligned} \tag{6}$$

According to Eq. (5) no coincidences are expected, while in Eq. (6) the terms in which each photon exit to different path do not cancel out and we have a coincidences probability of $p_{c,d} = \frac{1}{2}$. The expected visibility is then $V_{\Phi^+\Phi^+}^{th} = 1 - 2p_{c,d} = 1$ and $V_{\Phi^+\Phi^-}^{th} = 0$, these are in agreement with the measured behaviours reported in Fig. 5 (c,d).

Moreover, we analyze also the case when interfering input states are neither equal nor orthogonal. Let us consider to income on the input q-plates with polarization $|R\rangle_a$ and $|H\rangle_b$. In the first arm the generated state is $|L,-2\rangle_a$, while a VV state $|\Phi^+\rangle_b$ is generated in the second arm. Tacking into account the BS transformation, the output beam result to be:

$$\begin{aligned}
&\frac{1}{2}(\hat{c}_{L,-2}^\dagger - \hat{d}_{R,2}^\dagger)(\hat{c}_{R,2}^\dagger + \hat{d}_{L,-2}^\dagger + \hat{c}_{L,-2}^\dagger + \hat{d}_{R,2}^\dagger)|0,0\rangle_{cd} = \\
&= \frac{1}{2\sqrt{2}}(\sqrt{2}|L,-2\rangle_c |L,-2\rangle_c + |L,-2\rangle_c |R,2\rangle_c + \\
&\quad + |L,-2\rangle_c |L,-2\rangle_d - |R,2\rangle_c |R,2\rangle_d - \\
&\quad - |R,2\rangle_d |L,-2\rangle_d - \sqrt{2}|R,2\rangle_d |R,2\rangle_d)
\end{aligned} \tag{7}$$

In this condition the probability of having both photons on the same output is $p_{c,c} + p_{d,d} = \frac{3}{4}$ while the probability of having the photons come out of different outputs is $p_{c,d} = \frac{1}{4}$. Therefore, we expect an HOM visibility of $V_{R,H}^{Th} = \frac{1}{2}$, which is consistent with the experimental one reported in the Main Text.

Supplementary Note 2. EFFICIENCY ESTIMATION

In this section, the transmission of all optical components are reported to estimate the efficiency of the experimental platform. The single-photon countrate $C^{te} = 4$ MHz is measured at the output of the Q-Fiber (Quandela) module with an Avalanche Photo-Diode (APD) detector with $\eta_{det} \sim 38\%$ efficiency. Knowing the QD source is pumped with a 79 MHz-pulsed laser ($R_{exe} = 79$ MHz) and accounting for the limited efficiency of the APD, we can derive the fibered brightness of the single-photon source $\eta_{fibered} \sim 13.3\%$. The Q-Fiber module is connected to the experimental platform through optical fibers. Each connection is made with FC/PC mating sleeves, which each have a transmission of $\eta_{connector} \sim 80\%$, while the fiber-BS employed in the *inter*-particle regime has an insertion loss of $\eta_{BS} \sim 0.75$. The single-photon are then filtered in polarization with polarizing beamsplitters (PBS) and, since there is a residual of vertical polarized photons generated by the QD, the efficiency is $\eta_{pol} \sim 83\%$. The major sources of losses are the q-plates which have an efficiency of $\eta_{q-plate} \sim 70\%$ and the coupling of a VV beam converted to gaussian mode with a SMF $\eta_{coupling} \sim 45\%$. In conclusion, the overall efficiency of the generation stage is $\eta_{gen,1} = \eta_{fibered} \eta_{connector}^2 \eta_{pol} \eta_{q-plate} = 4.95\%$ and $\eta_{gen,2} = \eta_{fibered} \eta_{connector}^3 \eta_{BS} \eta_{pol} \eta_{q-plate} = 2.97\%$ respectively for *intra*- and *inter*-particle regime, while the tomography setup results to have an efficiency of $\eta_{tomo} = \eta_{q-plate} \eta_{coupling} \eta_{det} = 11.97\%$. Using such approximated efficiency, it is possible to estimate the expected signals in the different configurations of the experiment. For the *intra*-particle entanglement, all the measurements are performed on single events, and by taking into account the 50% loss due to the second beamsplitter (BS) of the interferometer, the expected generation rate is $R_{intra}^{gen} = \frac{\eta_{gen,1} R_{exe}}{2} = 1.96$ MHz, while the detected countrate should be $R_{intra} = \eta_{tomo} R_{intra}^{gen} = 234.1$ kHz. On the other side, in the *inter*-particle experiment, the measurements are performed detecting the coincidence counts, therefore the expected generation rate is $R_{inter}^{gen} = \frac{\eta_{gen,2} R_{exe}}{4 \cdot 2} = 8.71$ kHz while the detected coincidence rate is $R_{inter}^{gen} = \eta_{tomo}^2 R_{inter}^{gen} = 124.8$ Hz, where the coefficients $\frac{1}{4}$ and $\frac{1}{2}$ are due to the first and second BS of the interferometer, respectively.

η_{fibered}	$\eta_{\text{connector}}$	η_{BS}	η_{pol}	$\eta_{\text{q-plate}}$	η_{coupling}	η_{det}	$R_{\text{intra}}^{\text{gen}}$ (MHz)	R_{intra} (kHz)	$R_{\text{inter}}^{\text{gen}}$ (kHz)	R_{inter} (Hz)
13.3%	80%	75%	83%	70%	45%	38%	1.96	234.1	8.71	124.8

Supplementary Table 1. **Efficiency estimation:** The table showcases the experimental efficiency estimated for each loss of the apparatus. η_{fibered} represents the overall transmission efficiency of the single-photon source, including excitation laser rejection and extraction system losses. $\eta_{\text{connector}}$ is the transmission efficiency of single-mode optical fiber, η_{BS} the insertion loss of the fiber-BS, while $\eta_{\text{q-plate}}$ and η_{coupling} are the main losses of the implemented experimental platform due to the limited conversion efficiency of OAM modes and the higher divergence to which beams endowed with orbital angular momentum are subjected. Finally, η_{det} is the intrinsic efficiency of the Avalanche Photo-Diode detectors employed. Using these values the expected generated and detected count rates are evaluated for both the *intra-* ($R_{\text{intra}}^{\text{gen}}$ and R_{intra}) and *inter-*particle ($R_{\text{inter}}^{\text{gen}}$ and R_{inter}) regime.